International Journal of Mechanical Sciences 52 (2010) 777–783

Contents lists available at ScienceDirect

International Journal of Mechanical Sciences

journal homepage: www.elsevier.com/locate/ijmecsci

Collisions between two nonlinear deformable bodies stated within Continuum Mechanics

Fernando S. Buezas [a,b,*], Marta B. Rosales [b,c], Carlos P. Filipich [d]

[a] Department of Physics, Universidad Nacional del Sur, 8000 Bahía Blanca, Argentina
[b] CONICET, Argentina
[c] Department of Engineering, Universidad Nacional del Sur Alem 1253, 8000 Bahía Blanca, Argentina
[d] CIMTA - Centro de Investigaciones en Mecánica Teórica y Aplicada, FRBB, Universidad Tecnológica Nacional, 11 de Abril 465, 8000 Bahía Blanca, Argentina

ARTICLE INFO

Article history:
Received 19 October 2009
Received in revised form
30 December 2009
Accepted 8 January 2010
Available online 25 January 2010

Keywords:
Deformable bodies
Unilateral contact
Impact contact time
Lagrangian description

ABSTRACT

The study of the interaction between two deformable bodies that collide is of great interest since desired effects, as a stable contact, or undesired ones, as the failure of a mechanical part, can be predicted. In this work, a Signorini type contact model with impact considering large rotations and deformations is addressed. The problem is stated using the Continuum Mechanics formulation in two and three dimensions with the *Lagrangian* description employing the two Piola–Kirchhoff stress tensors with linear or non-linear constitutive equations. The governing equations are solved through a general purpose software oriented to solve partial differential equations by means of a finite element discretization. The impact of a deformable body over a rigid boundary or over other deformable body is tackled. Also a three-dimensional problem is addressed (i.e. a spheric ball impacting on a rigid surface). Numerical illustrations include parametric studies on the energy, the impulse forces and the time of contact for different initial conditions and materials. A comparison among the models is shown. Additionally the problem of the impact of two deformable solid balls is solved and contrasted with simpler models developed by other authors.

1. Introduction

The classical theory of contact in Mechanics beginning with Hertz in 1881 (see, for instance, Landau and Lifshitz [1]) is restricted to frictionless surfaces and perfectly elastic solids undergoing small deformations. By the second half of the past century, important progress was achieved to overcome these restrictions. A correct statement of the friction phenomenon has permitted the extension of the elastic theory to the sliding and friction of rolling elements. At the same time, the linear visco-elastic and plasticity theories have contributed to address deformations and stresses when inelastic bodies are in contact. Reference books including modern approaches in this field are Gladwell [2] and Johnson [3]. In more specific cases dealing with contact between very hard and soft bodies, such as glass and rubber surfaces, slipping noise phenomena are studied using stress waves considering the coupling of adhesion and unilateral contact among matrix/fiber interfaces with applications to composite materials [4,5]. Diverse friction regimes were addressed by Challen and Oxley [6]. A comprehensive review on articles dealing with mathematical, numerical and computational issues within Contact Mechanics may be found in Raous et al. [7]. On the other hand, very precise experiments can be carried out with available material in any undergraduate physics laboratory, for example, the functional relationship between the time of contact, the velocity of incidence and the length of a bar [8] or the validation of Hertz's theory in an inelastic collision [9] as well as the differences between bouncing springs, spheres and rods [10].

In this work, the contact problem between deformable bodies is tackled within the Continuum Mechanics formulation. The Signorini problem is stated together with the governing elasticity equations using the *Lagrangian* description. A general propose software is employed to discretize the spatial domain with a finite element approach.

Several illustrations include the study of the collision of two steel balls which is contrasted with a simpler model such as the well-known Hertz theory and experimental measures [11], a deformable spherical body impacting on a rigid surface, and a deformable disc impacting on a deformable body. From parametric studies, diverse results are obtained such as the time of contact, the velocity of incidence, energies, besides the basic variables (displacements at each point of the body). Functional relationships are derived and interesting conclusions may be

* Corresponding author at: Department of Physics, Universidad Nacional del Sur, 8000, Baha Blanca, Argentina. Tel.: +54 14595100; fax: +54 14595142.
E-mail address: fbuezas@gmail.com (F.S. Buezas).

0020-7403/$ - see front matter © 2010 Elsevier Ltd. All rights reserved.
doi:10.1016/j.ijmecsci.2010.01.003

drawn from their analysis. The comparison between different material models used in the present approach allows to define the validity of each constitutive law.

The motivation of the work reported here was to study the evolution of the contact force and energy in a head-on collision between two continuum bodies. It may be concluded that the above proposed approach presents the capability of dealing with arbitrary shaped bodies and materials governed by different constitutive equations.

2. Statement of the problem

This section contains theoretical issues such as the statement of the governing system (equations of motion and constitutive laws) and the description of the contact problem.

2.1. Equations of motion

Since the problem is stated in the *Lagrangian* or material reference, only the following equation has to be solved [12,13]:

$$\nabla_X \cdot \mathbf{P} + \rho_0 \mathbf{b} = \rho_0 \mathbf{A} \tag{1}$$

where $\mathbf{P}$ is the first Piola–Kirchhoff [13] stress tensor, $\rho_0 = \rho(\mathbf{X}, t_0)$ is the mass density of the initial configuration, $\mathbf{A} = \dot{\mathbf{V}} = \partial \mathbf{V}/\partial t = \partial^2 \mathbf{x}/\partial t^2$ is the acceleration field, $\mathbf{b}$ are the body forces and, $\mathbf{x}=\mathbf{x}(\mathbf{X},t)$ is the spatial position vector. ∇_X or $\nabla_X \cdot$ represents the gradient or the divergence with respect to the material coordinates $\mathbf{X}$ correspondingly. Within this frame, the boundary conditions are imposed on the initial boundary whose position is known by hypothesis:

$$\mathbf{x}(\partial V^1) = \bar{\mathbf{x}} \tag{2}$$

$$\mathbf{t}_0(\partial V^2) = \bar{\mathbf{t}}_0 \tag{3}$$

where $\mathbf{t}_0$ is the tension vector of Piola–Kirchhoff calculated for the rule $\mathbf{t}_0 = \mathbf{P} \cdot \mathbf{N}$. Thus, the problem at the boundary, as well as the initial conditions and the equations of motion, is fully stated. Once the differential problem is solved, both the position of the boundary and the location of any part of the body will be known for each instant.

The second Piola–Kirchhoff [13] stress tensor may also be useful. As is known, it is symmetric and is given by $\mathbf{P}=\mathbf{FS}$ where $[\mathbf{F}]_{ij} = \partial x_i/\partial X_j$ is the deformation gradient tensor, x_i is the i th component of the current position vector (spatial description), x_j is the j th component of the reference position vector (material description), $\mathbf{X}$. Then, the equations of motion can be rewritten as follows:

$$\nabla_X \cdot (\mathbf{FS}) + \rho_0 \mathbf{b} = \rho_0 \mathbf{A} \tag{4}$$

The next relationship relates $\mathbf{P}$, $\mathbf{S}$ and $\boldsymbol{\sigma}$ (the Cauchy stress tensor—spatial description)

$$\mathbf{F} \cdot \mathbf{S} = (\det \mathbf{F}) \boldsymbol{\sigma} (\mathbf{F}^{-1})^T = \mathbf{P} \tag{5}$$

2.2. Constitutive equations

In this work, we will deal with elastic materials which satisfy

$$\mathbf{S} = g(\mathbf{E}) \tag{6}$$

where g is a certain tensorial function, and

$$[\mathbf{E}]_{ij} = \frac{1}{2}\left(\frac{\partial u_i}{\partial X_j} + \frac{\partial u_j}{\partial X_i} + \frac{\partial u_k}{\partial X_i}\frac{\partial u_k}{\partial X_j}\right)$$

is the *Lagrangian* finite strain tensor (also known as Green–St. Venant [14]) and $\mathbf{u} = \mathbf{x}(\mathbf{X}, t) - \mathbf{X}$ is the displacement vector. In particular, the following constitutive law is proposed:

$$\mathbf{S} = \lambda \,\mathrm{tr}(\mathbf{E})\mathbf{I} + 2\mu\mathbf{E} \tag{7}$$

where λ and μ are constants. This law is also known as St. Venant–Kirchhoff material model [15].

A simple and interesting model of a hyperelastic material is given by the following non-linear relationship:

$$\mathbf{S} = \mu(\mathbf{I} - \mathbf{C}^{-1}) + \lambda(\ln J)\mathbf{C}^{-1} \tag{8}$$

that describes a Neo-Hookean compressible solid. Again λ and μ are constant, $\mathbf{C} = \mathbf{F}^T \cdot \mathbf{F}$ is Green's deformation tensor and $\mathbf{J}$ = det($\mathbf{F}$). Moreover, if J=1 in Eq. (8), a Neo-Hookean incompressible solid is modeled.

2.3. Unilateral contact

The contact model between two deformable bodies to be employed in this work will be described in what follows. As a first approach to the contact model, let us suppose that a deformable body interacts with a rigid and fixed obstacle.

The contact condition is that the deformable body does not penetrate in the rigid obstacle.

Let a body B occupy the domain Ω in a two- or three-dimensional space (Fig. 1). The body boundary $\Gamma = \Gamma_F \cup \Gamma_D \cup \Gamma_C$ is smooth enough and is in contact with a rigid fixed body. Part Γ_F of the boundary Γ corresponds to the boundary region at which the stresses are prescribed (natural conditions to the problem (1)). Γ_D is the region where the displacements are prescribed (geometric conditions) and Γ_C, where there is a contact with the rigid body. There, the displacements $\mathbf{v}=\mathbf{x}_B - \mathbf{x}_R$ are the difference between the coordinate of the point at the deformable body boundary and the corresponding one at the rigid boundary (see Fig. 1). The Signorini problem (unilateral contact) is stated as follows (subscript N denotes the normal direction):

$$v_N \le 0, \quad t_{cN} \le 0, \quad u_N \, t_{cN} = 0 \tag{9}$$

(1) No contact $\Rightarrow v_N \le 0$ and $t_{cN} = 0$.
(2) Contact $\Rightarrow v_N = 0$ and $t_{cN} \le 0$.

Conditions (9) constitute a non-continuous or non-smooth problem since tc_N is a multi-valuated application of the v_N field (or simply, tc_N is not a function of v_N). From the Analytical Mechanics viewpoint [16], Signorini conditions result in a non-holonomic constrained problem due to the inequalities. This is reflected in the fact that neither the stresses nor the contact surface is known before solving the problem. If it were solved, the deformation could be calculated but they are necessary to the classical statement of the boundary. In other words, in Continuum Mechanics, the boundary conditions have to be previously known to solve the problems. However, the Signorini problem gives the boundary conditions an unknown character.

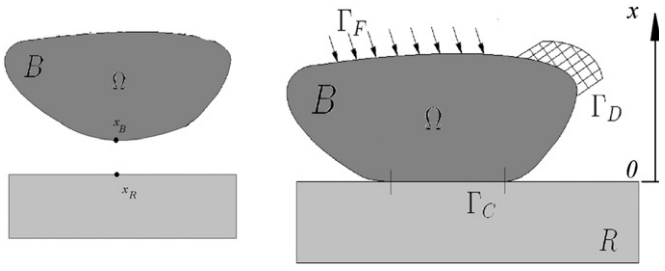

Fig. 1. Scheme of the contact between a deformable body against a rigid contact.

The contact law (9) is non-holonomic, since no regular restriction given by an equality exits. Instead, the problem contains a restriction given by a set of inequalities. Furthermore, when contact appears, neither the stress value nor the displacement is defined. This alternation between natural and geometric conditions gives the problem the non-regular character since the moment in which each one stands is also an unknown. The regularization of the contact problem consists in the replacement of the rigid condition (9) by a smooth or regular one. The non-holonomic problem is replaced by a problem without constraint. The boundary condition will be always natural, by imposing a functional relationship between stresses and displacements, i.e. the problem is regularized by means of the following function:

$$t_{cN} = \begin{cases} -k(v_N)^m & \text{if } v_N > 0 \\ 0 & \text{if } v_N \le 0 \end{cases} \tag{10}$$

where k is a sufficiently large number in order for (10) to approximate (9) and m is an arbitrary constant ($m=1$ for the linear approximation).

2.3.1. Extension to the contact between two deformable bodies

When dealing with infinitesimal strains and displacements, the contact problem is easily solved by introducing a change of variable in the Signorini problem (9) which is now double

$$\text{BODY B1} \begin{cases} d(x_1,x_2) \ge 0 \\ t_{cN1} \le 0 \\ x_1\ t_{cN1} = 0 \end{cases} \quad \text{and} \quad \text{BODY B2} \begin{cases} d(x_2,x_1) \ge 0 \\ t_{cN2} \le 0 \\ x_2 t_{cN2} = 0 \end{cases} \tag{11}$$

where $d(x_1,x_2)$ and $d(x_2,x_1)$ are both the distance between x_1 (B1) and x_2 (B2). When infinitesimal displacements are assumed, then unit vectors satisfy $\mathbf{N}_2 = -\mathbf{N}_1$ and the pair of points x_1 and x_2 are known before the problem is solved, and are located on the normal to each surface. Instead, if the displacements or strains are considered finite, there is no knowledge about which pair of points will contact, neither about the corresponding normal unit vectors. In this case, the minimum of the distances between all possible pairs of points has to be evaluated as well as the corresponding unit normal vectors:

$$\begin{cases} \min(d(x_1,x_2)) \ge 0, \\ t_{cN1} \le 0, \\ x_1 t_{cN1} = 0, \end{cases} \quad \begin{cases} \min(d(x_2,x_1)) \ge 0 \\ t_{cN2} \le 0 \\ x_2 t_{cN2} = 0 \end{cases} \tag{12}$$

3. Computational simulations

Sections 3.1 and 3.2 describe the numerical scheme implemented to solve the equations of motion. Next, Sections 3.3–3.5 include the following examples: a collision between a deformable sphere against a rigid plane, a deformable disk impacting on both, a deformable and a rigid body and finally, the impact between two deformable spheres.

3.1. Equations of motion in weak form

It is very simple to get the weak formulation of equations of motion. Let $\mathbf{W}$ be any vector field of variables referred to the body in its nondeformed configuration (material coordinates or *Lagrangian* description). Multiplying the equations of motion by $\mathbf{W}$ and integrating over V_0 we get

$$\int\int\int (\nabla_X \cdot \mathbf{P} + \rho_0 \mathbf{b} - \rho_0 \mathbf{A}) \cdot \mathbf{W}\, dV_0 = \mathbf{0} \tag{13}$$

$$\int\int\int_{\partial V} (\mathbf{t}_0 \cdot \mathbf{W})\, dA_0 + \int\int\int [\rho_0(\mathbf{b}-\mathbf{A}) \cdot \mathbf{W} - \mathbf{P} \cdot \nabla_X \mathbf{W}]\, dV_0 = 0 \tag{14}$$

where (14) is obtained after integrating (13) by parts (using Gauss theorem). Remember that (∇_X) indicates the gradient and $(\nabla_X \cdot)$ the divergence with respect to the X coordinate.

The surface integral is divided into two parts. Suppose that the displacement $\mathbf{u}$, and consequently the velocity $\mathbf{V}$, is prescribed in a part of the boundary's surface (Γ_D in Fig. 1) and the stress is given in the other part (Γ_F in Fig. 1). In order to incorporate the boundary conditions (2) and (3)

$$\mathbf{x}(\partial V^1) = \overline{\mathbf{x}}$$

$$\mathbf{t}_0(\partial V^2) = \overline{\mathbf{t}}_0$$

in the weak form (14), the first trial functions $\mathbf{W}$ are assumed null in Γ_D. Then the surface integral in Eq. (14) reduces to

$$\int\int_{\partial V_0} (\mathbf{t}_0 \cdot \mathbf{W})\, dA_0 = \int\int_{\Gamma_F} (\mathbf{t}_0 \cdot \mathbf{W})\, dA_0 = \int\int_{\Gamma_F} \overline{\mathbf{t}}_0 \cdot \mathbf{W}\, dA_0$$

Finally, the weak formulation consists of the following relations:

$$\int\int_{\Gamma_F} (\mathbf{t}_0 \cdot \mathbf{W})\, dA_0 = \int\int\int [\rho_0(\mathbf{b}-\mathbf{A}) \cdot \mathbf{W} - \mathbf{P} \cdot \nabla_X \mathbf{W}] dV_0 \tag{15}$$

$$\mathbf{x} = \overline{\mathbf{x}} \text{ on } \Gamma_D \tag{16}$$

$$\mathbf{x}(\mathbf{X}, t_0) = \mathbf{x}_0(\mathbf{X}) \quad \text{and} \quad \dot{\mathbf{x}}(\mathbf{X}, t_0) = \mathbf{V}_0(\mathbf{X}) \tag{17}$$

3.2. Galerkin method and discretizations in polynomial elements

Let the function $\mathbf{u}$ be expanded in a series of $\boldsymbol{\phi}_i(\mathbf{X})$

$$\mathbf{u}(\mathbf{X}, t) \simeq \sum_{i=1}^{N} \boldsymbol{\phi}_i(\mathbf{X}) c_i(t) \tag{18}$$

here $c_i(t)$ are functions only of time. The polynomials

$$\boldsymbol{\phi}_i(\mathbf{X}) = [\phi_{x_1 i}(\mathbf{X}), \phi_{x_2 i}(\mathbf{X}), \phi_{x_3 i}(\mathbf{X})]^T$$

are functions with the same features as $\mathbf{W}$. Every $\phi_i(X)$ is null outside the domain i which is defined. For each i th cell or element, the polynomial $\phi_i \neq 0$ and the remainder $\phi_j = 0$ for each $j \neq i$. The set of all polynomials ϕ_i generate the space of solutions of the differential problem.

Replacing Eq. (18) in (1) and integrating on the whole domain:

$$\int\int\int \left[\nabla_X \cdot \mathbf{P}(\mathbf{u}) + \rho_0 \mathbf{b} - \rho_0 \left(\sum_{i=1}^{N} \boldsymbol{\phi}_i(\mathbf{X}) \ddot{c}_i(t) \right) \right] \cdot \boldsymbol{\phi}_i(\mathbf{X}) dV_0 = 0 \tag{19}$$

where $\mathbf{P}(\mathbf{u})$ means that Piola–Kirchhoff stress tensor is calculated from $\mathbf{u}(\mathbf{X},\mathbf{t})$ through constitutive relations (7) or (8).

At last, integrating by parts in the general sense, that is using the theorems of vectorial calculus (Gauss, Stokes or Green theorems) we get

$$\int\int_{\partial V_0} (\mathbf{t}_0(\mathbf{u}) \cdot \boldsymbol{\phi}_i)\, dA_0 + \int\int\int \left[\rho_0 \left(\mathbf{b} - \sum_{i=1}^{N} \boldsymbol{\phi}_i \ddot{c}_i \right) \cdot \boldsymbol{\phi}_i(\mathbf{X}) - \mathbf{P}(\mathbf{u}) \cdot \nabla_X \boldsymbol{\phi}_i \right] dV_0 = 0 \tag{20}$$

This task was performed with the help of FlexPDE software [18] which is a scripted finite element model builder and a numerical solver with the following features:

1. The user introduces the governing system as well as definitions, geometry and all the necessary information of the model. FlexPDE software uses standard Galerkin finite element methods. Quadratic interpolation over triangles or tetrahedra

was used in the present work. Nodal values are placed on corners and sides of the mesh cells, so that all solutions are continuous throughout space.
2. The Galerkin equations are formed by symbolic analysis, which substitutes definitions, segregates dependencies on variables, applies integration by parts, integrates over cells, and ultimately differentiates the resulting system with respect to system variables to form the coupling matrix.
3. Equations are solved simultaneously by a conjugate-gradient iterative method. Nonlinear systems automatically apply a Newton–Raphson iteration process with backtracking. This results in a fully implicit solution at the end of each grid phase.
4. Time-evolution equations apply an implicit backward difference method for integration in time that is stiffly stable. Variables are approximated by quadratic polynomials in time, and the timestep is controlled to keep the cubic term smaller than the required error.
5. The finite element equations minimize the residual of the Galerkin integral over a patch of cells surrounding each mesh node. Then the residuals in each cell are analyzed independently as a measure of compliance, and each cell in which the required error tolerance is exceeded, is subdivided.

3.3. Collisions between two identical deformable steel balls

Hessel et al. [11] proposed a simple model based on the Hertz theory to describe and fit experimentally the contact of two steel spheres. The authors found that the experimental results agree with Hertz's theory of contact [1]. We propose the modeling of spheres of identical size and characteristics as that studied by Hessel et al. The problem consists of two identical steel balls with diameter d=0.0381 m and mass m =0.2258 kg. Fig. 2 shows the collision time as a function of velocity v. In this simulation, the law of Δt as a function of the impact velocity corresponding to identical steel balls, i.e. $\Delta t = 2.94(\mu^2/k^2 v)^{1/5}$ where $\mu = m/2$ and $k = 4/(5D)\sqrt{R/2}$, R is the radius of the sphere and D=3/(2E), for the characteristics used in this example, is reduced to $\Delta t = 1.18567 \times 10^{-4}/\sqrt[5]{v}$ or $\Delta t = \alpha v^{\gamma}$. Hessel et al. fit the value of the coefficient and the exponent of this expression from experimental measurements. Table 1 indicates the values of the coefficients reported in [11], with Hertz theory and the ones calculated with the present model. In Fig. 2 and Table 1 it can observed that the coincidence among the three approaches is evident and are within the expected uncertainty of any practical

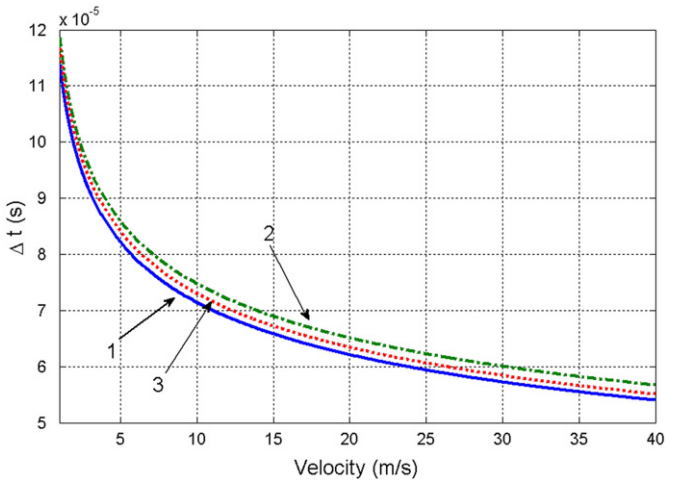

Fig. 2. The collision time as a function of the velocity. 1 — Hertz. 2 — Hessel et al. 3 — Present study.

Table 1
Comparison of values of coefficients found by Hessel et al., with Hertz's theory and the ones calculated with the present study.

	Hessel et al. [11]	Hertz's [1]	Present work
α	$(1.138 \pm 0.002) \times 10^{-4}$	1.1857×10^{-4}	1.1672×10^{-4}
γ	-0.202 ± 0.002	-0.2	-0.2035

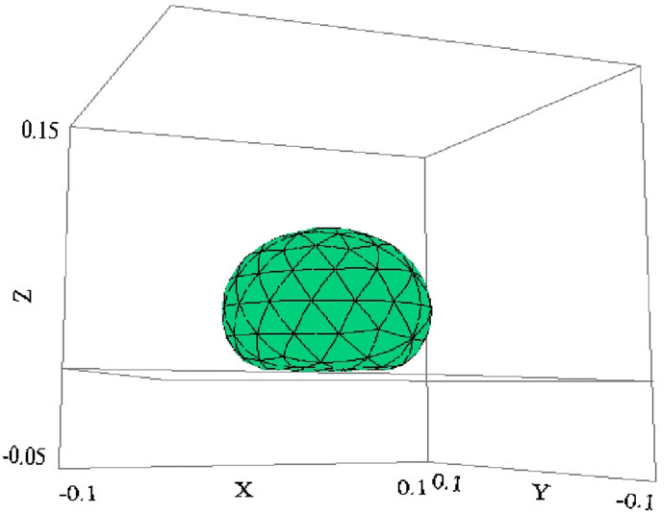

Fig. 3. Snapshot of the collision of a three-dimensional sphere against a rigid boundary.

experiment. It should be noted that, in this example, we are dealing with a collision of steel balls at low impact velocity and consequently, only small deformations are involved. As is expected, this model contains the Hertz theory and experimental results of Hessel et al. in the case of small deformations. In the following sections we will show cases of collisions in which the Hertz theory is not applicable because of the large deformations and other material laws.

3.4. Deformable spherical body impacting on a rigid surface

The material of the spherical body is modeled with the constitutive Eq. (7) assuming $E = 7 \times 10^6\,\mathrm{Nm}^{-2}$ and $\nu \to 0.5$ were $\lambda = \nu E/(1+\nu)(1-2\nu)$, $\mu = E/2(1+\nu)$ and mass density $\rho = 1722\,\mathrm{kg/m}^3$. This material is chosen for two reasons: firstly, some previous simple test (not reported here) was performed on a rubber ball and it was found that the material characteristics yield in this range (similar to the values reported by Eringen [17]). Secondly, a soft material, as the one herein proposed, makes more complex phenomena due to large deformations apparent. Fig. 3 depicts the ball at its maximum deformation. The radius of sphere is r=0.05 m. The initial condition is v=8 m/s normal to the rigid body. The time of contact is, in this case, t=0.00603 s.

The adaptive time step is tested and controlled by checking the energy which is constant since we are dealing with a conservative impact. This energy is

$$E_T = T + U_e + U_g \tag{21}$$

where $T = \frac{1}{2}\int\int\int \rho_0 \mathbf{V}\cdot\mathbf{V}\,dV_0$; $U_g = g\int\int\int \rho_0 y\,dV_0$; $\dot{U}_e = \int\int\int \mathrm{tr}(\mathbf{S}\cdot\dot{\mathbf{E}})\,dV_0$ are the total kinetic, gravitational and elastic energies, respectively, and dV_0 is the element of volume. Here $\dot{U}_e$ stands for the elastic power. It can be proved that for the constitutive law (7) and (8), it takes the form of the elastic energy as

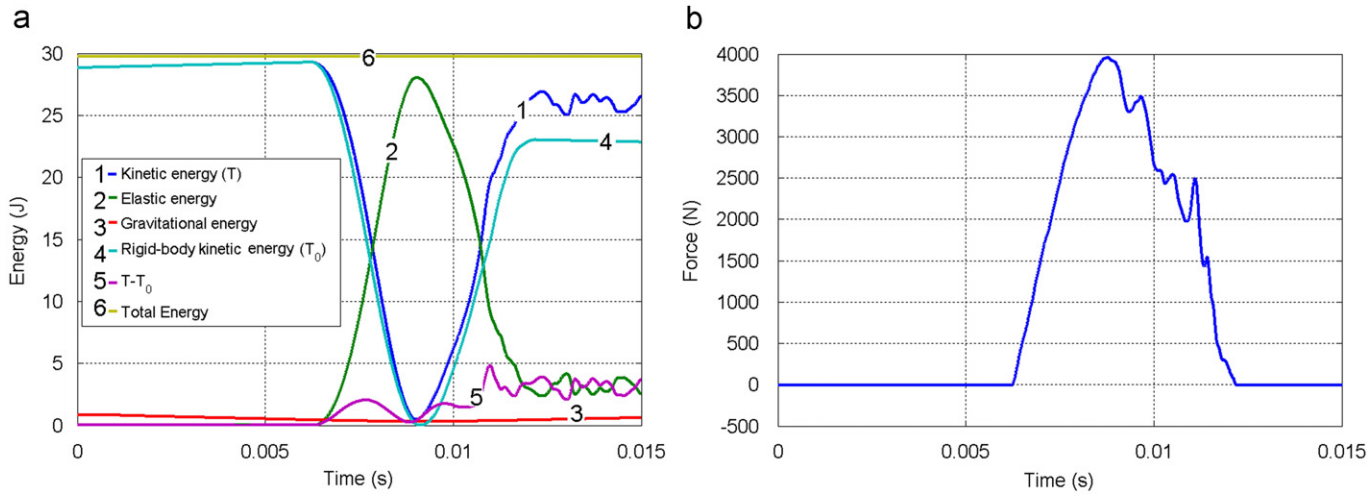

Fig. 4. Spherical ball impacting on a rigid boundary. Energy (in Joules) and impact force (in Newtons) as functions of time.

$U_e = \lambda/2(\mathrm{tr}(\mathbf{E}))^2 + \mu\mathrm{tr}(\mathbf{E}\cdot\mathbf{E})$ and $U_e = \mu/2[\mathrm{tr}(\mathbf{C})-3] - \mu\ln J + \lambda/2(\ln J)^2$, respectively. It is interesting to make a partition of the kinetic energy into a vibration term $(T-T_0)$ and a *rigid-body* term

$$T_0 = \tfrac{1}{2}M\mathbf{V}_{CM}^2$$

where M is the total mass of the sphere and $\mathbf{V}_{CM}$ is the velocity of its center of mass (which must remain constant except for gravitational deceleration once contact has stopped) (Fig. 4a). This partition is of interest because in a real material (and hence somewhat internal dissipative), the vibration energy will eventually decay to zero, and this is a contribution to what is commonly known as the *coefficient of restitution*. There are other sources of energy dissipation such as radiation of sound through the boundary of the sphere, and the wave propagation of the target itself (here a rigid boundary).

Fig. 4b depicts the variation of the impact force with time. The acceleration of the center of mass can be calculated as $\mathbf{A}_{CM} = 1/V_0 \int\int\int \mathbf{A}(\mathbf{X},t)\,dV_0$ where V_0 is the non-deformed volume of the body. Approximately 9×10^{-3} s after starting the collision, a series of oscillations in the rebound force can be observed. This is, probably, due to the time the elastic wave takes to pass through the sphere and to return to the point of contact with the rigid body.

3.5. Deformable disc impacting on a deformable body

Dealing with the impact of a deformable body against another adds complexity to the problem since the positions of points of each boundary that will contact are unknown. Here, Eq. (12) should be employed at the cost of increasing the CPU time. Not only the body boundary trajectories but also the minimum distance at each instant of time have to be monitored.

In this example, the disc of radius $r=0.5$ m impacts on a body with dimensions $10\,\mathrm{m}\times 2\,\mathrm{m}$ both with identical elastic characteristics. The second body is not externally restricted. Neither friction nor gravitational forces were considered and the governing constitutive law (7) was stated with $E = 7\times10^6\,\mathrm{Nm}^{-2}$, $\nu\to0.5$ and $\rho = 1722\,\mathrm{kg\,m}^{-3}$. The initial conditions of the disc are the velocity of incidence $v=10$ m/s with normal direction to the other body, which is at rest. After the collision, the disc is reflected and the prismatic body is directed downwards. Finally, the variations of the energy are displayed in Fig. 5. The variation for the disc energy is shown in Fig. 5a, the time history of prismatic body energy is shown in Fig. 5b, and the total energy (disc + prismatic body) in Fig. 5c. Since the system is conservative, the total energy should remain constant. This feature is used to test the numerical convergence of the solutions. In this figure we can see how, when the impact ends, the rigid-body part of kinetic energy (T_0) is only 30% of the initial one. Again, the rest is vibrational kinetic energy $(T-T_0)$ and would decay to zero if any dissipation were considered. Now, not only the disc is vibrating, but also the prismatic body. Finally, Fig. 5d shows a snapshot of the interaction of the system at its maximum deformation (i.e. $t=0.04$ s).

Let us now consider the particular case of the disc impacting on a rigid surface, assuming the same data as before. An interesting issue in this study is the determination of the time the bodies remain in contact which can be estimated by observing when the force $\mathbf{F}(t) = \int\int\int \mathbf{A}(\mathbf{X},t)\rho_0\,dV_0$ is not null.

The examples were run for two different material (Eqs. (7) and (8)). A parametric study was performed varying the impact velocity and calculating 10 cases per unit of velocity. Fig. 6 shows a graphic of the time of contact vs. the initial velocity. It can be observed that the behavior is monotonically decreasing, in a similar fashion to the Hertz curve. In all the cases, the Neo-Hookean material yields lower impact times than the St. Venant–Kirchhoff material. The constants involved in both models were chosen such that in the small deformation range, both reproduce the same Hookean constitutive models. Thus, for very low impact velocity the curves are asymptotic. The elastomeric constitutive model demands larger computational times. It can be concluded that the general trend is that the time of contact decreases as the impact velocity increases. Fig. 7 shows the variation of the impact force with time for the two material models. Fig. 7a represents the case of a low impact velocity ($v=1$ m/s). Both materials behave similarly. A higher velocity case ($v=10$ m/s) is depicted in Fig. 7b. Here, the different response is apparent.

4. Conclusions

The impact of deformable bodies with contact has been addressed within the Continuum Mechanics stated in the *Lagrangian* reference. Geometric nonlinearities as well as linear and nonlinear constitutive laws were considered. Some issues, as the regularization of the contact problem, were tackled. The resulting nonlinear differential problem was solved with the help of a finite element discretization.

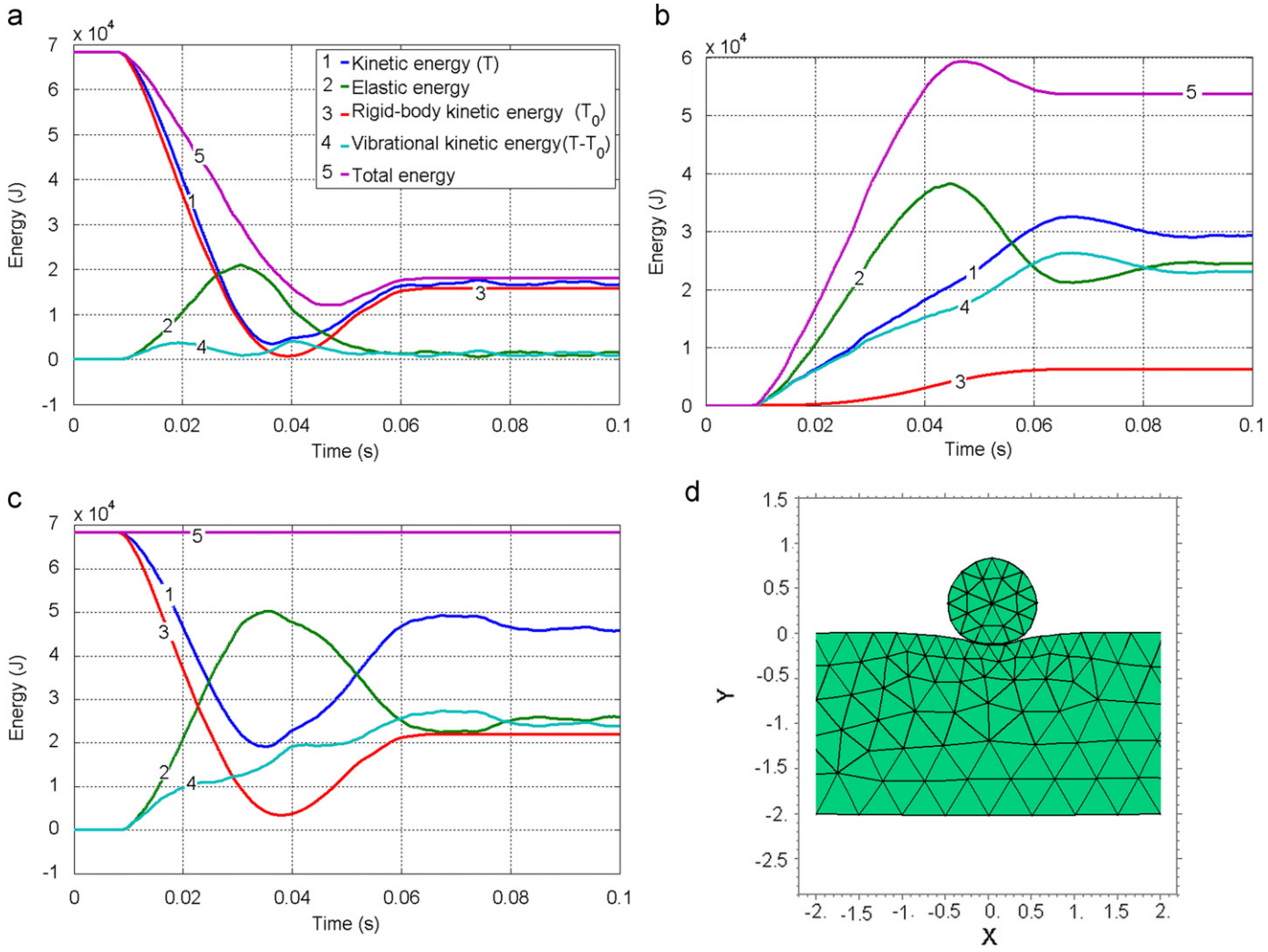

Fig. 5. Energy variations in the impact of two deformable bodies. (a) Only disc; (b) Only prismatic deformable body; (c) disc and prismatic deformable body and (d) snapshot of the interaction between the disc and the prismatic body.

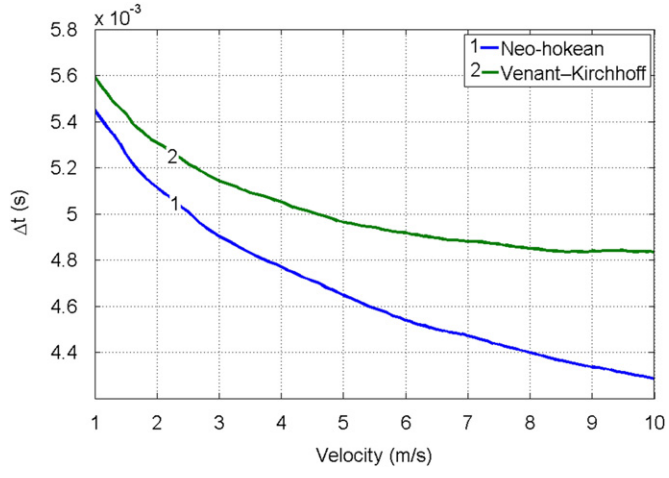

Fig. 6. Deformable disc impacting on a rigid body. Time of contact as a function of the initial velocity for a body governed by constitutive law (7) and with constitutive law (8).

The proposed formulation was applied to three problems. First, the collision of two steel balls was studied and from a comparison with other authors' approaches, it is concluded that, for this material and low impact velocity, the classical theory of Hertz and the present model are coincident. Otherwise, Hertz theory is not applicable. In the case of a deformable sphere impacting against a rigid body, an analysis of the energy components is useful, among other purposes, to estimate the coefficient of restitution. Also, the energy studies permit the monitoring of the solution quality when dealing with conservative problems. The temporal variation of the impact force allows observing a different behavior to the one foreseen by means of the Hertz theory. The peak variations of the force can be attributed to the wave propagation in the impacting deformable body. When dealing with the case of a deformable disc impacting on a deformable prismatic body, the components of the energy were also distinguished for each body and, as before, the coefficient of restitution can be inferred and also the complexity involved in the energy transfer from one body to the other. The parametric study of the time of contact as a function of the impact velocity was performed for the disc impacting on a rigid surface and with two constitutive laws, respectively. The general behavior is qualitatively similar to the Hertz theory since the time of contact decreases as the impact velocity increases. However, some smooth irregularities can be noticed. Since the calculations were made with high numerical precision, these particularities could not be attributed to a numerical noise interference but to the internal wave

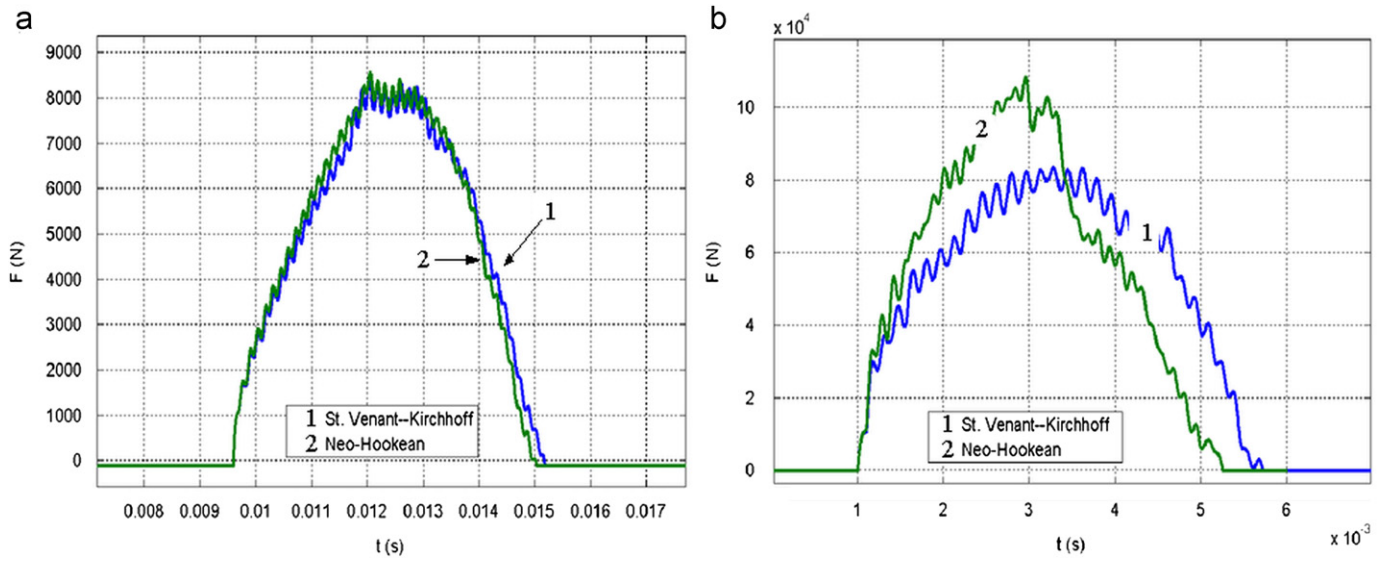

Fig. 7. Contact force during the impact of the disc using St. Venant–Kirchhoff and Neo-Hookean constitutive models. (a) Velocity of incidence v = 1 m/s; (b) Velocity of incidence v = 10 m/s.

propagation. It was also found that the Neo-Hookean material always yields lower impact times. The variation of the impact forces with time for the case of a disc considering two different material laws with low and high impact velocities shows that at a low velocity both materials behave similarly and at a higher velocity, the Neo-Hookean material exhibits stiffening with an increase of the maximum force and a lower time of contact.

Finally, the proposed approach can handle arbitrary shaped bodies and other material laws. More complex phenomena like finite deformation problems with friction were tackled in [19].

Acknowledgments

This work was supported by SGCyT-UNS and CONICET (Argentina). The authors would also like to thank the reviewer's suggestions and comments.

References

[1] Landau LD, Lifshitz EM. Theory of elasticity. In: Course of theoretical physics, vol 7. 3rd revised ed. London: Butterworth-Heinemann; 1995.
[2] Gladwell G. Contact problems in the classical theory of elasticity. Dordrecht: Kluwer Academic Publishers; 1980.
[3] Johnson KL. Contact mechanics. Cambridge: Cambridge University Press; 1987.
[4] Barbarin S. Instabilité et Frottement en Elasticit é, Application à un Problème de Ondes d' Contrainte. PhD thesis, Université de Provence, Marseille, France; 1997.
[5] Monerie Y, Raous M. A model coupling adhesion to friction for the interaction between a crack and a fibre/matrix interface. Zeitschrift f ür angew and te Mathematik und Mechanik 2000;80:205–8.
[6] Challen J, Oxley P. An explanation of the different regimes of friction and wear using asperity deformation models. Wear 1979;53:229–43.
[7] Raous MJ, Moreau J. Contact mechanics. Plenum Press; 1995.
[8] Britton WGB, Fendley JJ, Michael ME. Longitudinal impact of rods: a continuing experiment. American Journal of Physics 1978;46:1124.
[9] Gugan D. Inelastic collision and the Hertz theory of impact. American Journal of Physics 2000;68:920.
[10] Cross R. Differences between bouncing balls, springs, and rods. American Journal of Physics 2008;76:908.
[11] Hessel R, Perinotto AC, Alfaro RAM, Freschia AA. Force-versus-time curves during collisions between two identical steel balls. American Journal of Physics 2006;74:176.
[12] Gurtin ME. An introduction to continuum mechanics. New York: Academic Press; 1981.
[13] Wang C, Truesdell C. Introduction to rational elasticity. Dordrecht: Kluwer Academic Publishers; 1973.
[14] Truesdell C, Toupin R. The classical field theories. Berlin: Springer; 1960.
[15] Truesdell C, Noll W. The non-linear field theories of mechanics. Berlin: Springer; 2004.
[16] Goldstein H. Classical mechanics, 2nd ed. Reading, MA: Addison-Wesley; 1980.
[17] Eringen AC. Mechanics of continua. Huntington, NY: Robert E. Krieger Publishing Co.; 1980.
[18] PDE Solutions Inc, 2009. home page 〈http://www.pdesolutions.com/index.html〉.
[19] Buezas FS. Damage detection in mechanical—structural elements: modeling within non-linear mechanics including contact at the crack. PhD thesis, Universidad Nacional del Sur. Argentina; 2009 (in Spanish).